

Fault condition detection for a copper flotation process based on a wavelet multi-scale binary froth image

<http://dx.doi.org/10.1590/0370-44672015680195>

Lu Ming

Doctor, Central South University
School of Information Science and Engineering
Changsha - Hunan Province - China
mlu@hnust.edu.cn

Gui Wei-hua

Professor of Central South University
School of Information Science and Engineering
Changsha - Hunan Province - China
gwh@csu.edu.cn

Peng Tao

Professor of Central South University
School of Information Science and Engineering
Changsha - Hunan Province - China
lightxp99999@163.com

Cao Wei

Master, Central South University
School of Information Science and Engineering
Changsha - Hunan Province - China
37812588@qq.com

Abstract

Considering the difficulty of detecting the fault condition of copper flotation in real-time, a new fault condition detection method based on the wavelet multi-scale binary image is proposed. Firstly, the froth gray image is decomposed into approximation sub-images and detailed sub-images by wavelet transformation, whereby the approximation sub-images of different scales are restructured and binarized. Then a new feature that is directly related to froth morphology, namely the equivalent size feature, is obtained by calculating the white area of each binary image according to the space-frequency relationship of a two-dimensional wavelet transformation. After this, the equivalent size distribution of the froth image can be obtained through the equivalent size feature. At last, the equivalent size distributions of different froth images are compared in order to classify the froth images under different flotation conditions. Experiment results, together with the industrial field data, show that this method can simply and effectively detect fault conditions in the copper flotation process.

Keywords: copper flotation; fault working condition detection; wavelet multi-scale binary froth image; equivalent size feature.

1. Introduction

In the flotation process, any inappropriate operation or equipment failure can lead to a fault condition which will ultimately impact the flotation performance. For instance, inappropriate chemical-feeding, excessive air pressure or any disturbance factor in the flotation process will lead to froth abnormalities, such as hydration and viscosity, etc. Although the faulty condition is generally unlikely to result in the suspension of the flotation process, it can certainly influence the mineral grade, the recovery rate and so on (Aldrich C, 2010, REN H F *et al.*, 2011, YANG CH H *et al.*, 2009). Therefore, the timely and accurate detection of fault conditions is essential for the flotation process. However, the traditional method of detecting fault

conditions by the visual inspection of the froth surface fails to meet the demand of timeliness and accuracy for fault condition detection. With rapid development in computer vision and image processing technology, we have made great strides in finding an intelligent method for condition detection with respect to froth flotation features (GUI W H, 2014, Moolman D.W, Aldrich C, 1994). LIN Y.Q. *et al.* have established the PCA model based on the dynamic weight of texture element distribution and have further obtained the detection threshold according to the statistics of that model, which enables the timely detection of fault conditions in the flotation process (LIN YQ *et al.*, 2013). With the timely and accurate detection of fault conditions at the flotation site,

the flotation control system can adjust the production parameters in time, so as to keep the flotation process at the optimal condition.

Research shows that a morphological feature of foam is the comprehensive reflection of flotation conditions (CIT IR C *et al.*, 2004). An essential part of fault condition detection in flotation is to accurately extract the froth morphological feature that is closely related to production indices in flotation. The morphological features of froth including color, size, loading rate, velocity and stability, etc., which are traditionally applied in condition detection for copper flotation, are mainly obtained through image segmentation (YANG CH H *et al.*, 2009, Moolman D.W *et al.*, 1995), but

these features that are obtained directly through segmentation of the original image do not have the multi-scale property (J.M. Parts-Montalban *et al.*,2011, XU C H *et al.*,2012). A binary image is the simplest form for the characterization of an image. After a binary image of the froth grayscale image is made, statistics of the morphological features, such as froth number and bubble size, etc. can be obtained. Bao Lin *et al.* have set the segmentation threshold for a froth image based directly on their experience, so as to obtain a binary image of the froth. Having achieved this image, statistical analysis is done to obtain the bubble size distribution, and finally different flotation conditions are identified according to the different size distribution of the froth (Bao L, Bodil R,2008). Froth features obtained directly by binary froth imagery do not have a multi-scale property, like

those produced by image segmentation.

In contrast, wavelet analysis has the multi-scale property and can perform a multi-channeled time-frequency domain analysis of signals by simulation of the human vision system, so that more informative statistical froth features can be obtained. Gianni Bartolacci *et al.* adopted the wavelet multi-scale analysis to extract statistical features from froth imagery and used those features as texture descriptors to differentiate different types of froth (Bartolacci G *et al.*,2006). One scholar used the method of wavelet transformation to extract texture uniformity features, which helped to create a quantitative description of the surface texture of fine froth. The scholar also obtained the best texture range for fine froth through experimental analysis, so that any change of the flotation condition can be monitored in real time (TANG

ZH H,2011). Although the traditional image features extracted through wavelet analysis have the multi-scale property, it is difficult to adopt this method for the direct judgment of the onsite condition, due to its great difficulty in describing the morphological froth features that are easily recognizable for visual inspection in practice (Liu J J *et al.*,2005).

A wavelet multi-scale binary method is proposed in this paper for the feature extraction from the froth image. An equivalent size feature (the multi-scale statistical feature), which is directly related to froth morphology, is extracted by this method. And this feature is adopted to detect fault conditions including hydration froth and viscous froth, etc. in copper flotation so as to ensure that the overall flotation process is kept at the optimal condition by the timely adjustment of the production operation.

2. Description of fault conditions in copper flotation

Figure 1 shows the monitoring system for the working conditions of copper flotation. In this system, the froth video from the flotation site is captured by cam-

eras and thus used for real time monitoring of the working conditions.

As an important visual feature, bubble size can well reflect changes of

key production indices and technological parameters in the flotation process. As a result, it is effectively applied in fault condition detection for copper flotation.

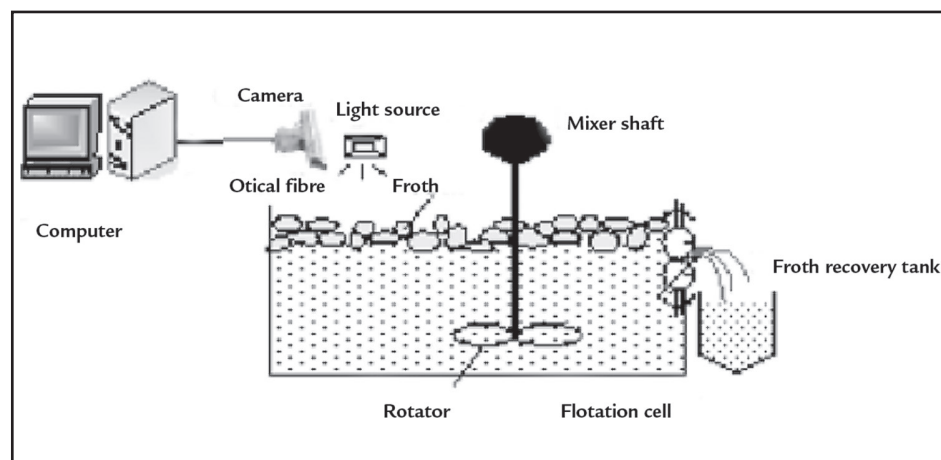


Figure 1
Sketch map of condition monitoring system in copper flotation

Figure 2 and figure 3 show respectively froth image under normal conditions and that under a fault condition from the copper flotation site.

Under normal conditions, the froth is of a moderate size and froths of different sizes are evenly distributed; the hydrated froths are mainly of small

sizes, with a relatively high mobility; the viscous froths are evenly distributed, of a relatively high viscosity and generally smaller than the normal ones.

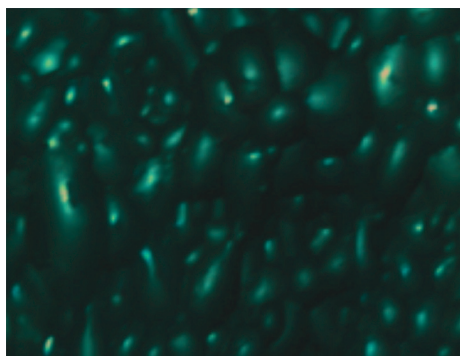
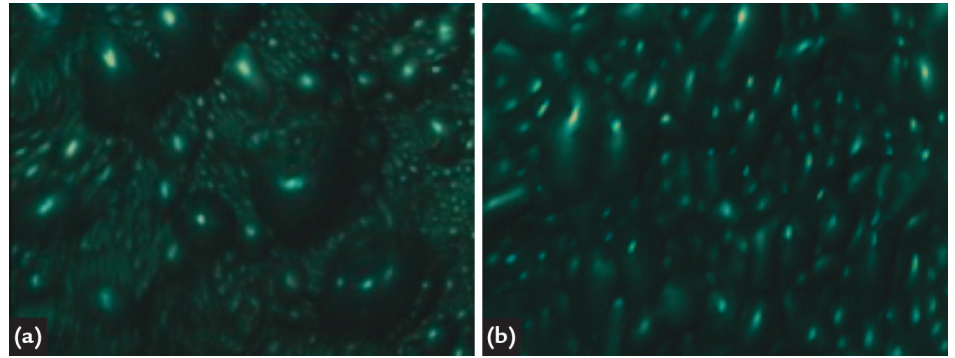


Figure 2
Froth image of normal condition

Figure 3
Froth images of fault condition
(a) Hydrated froth
(b) Viscous froth

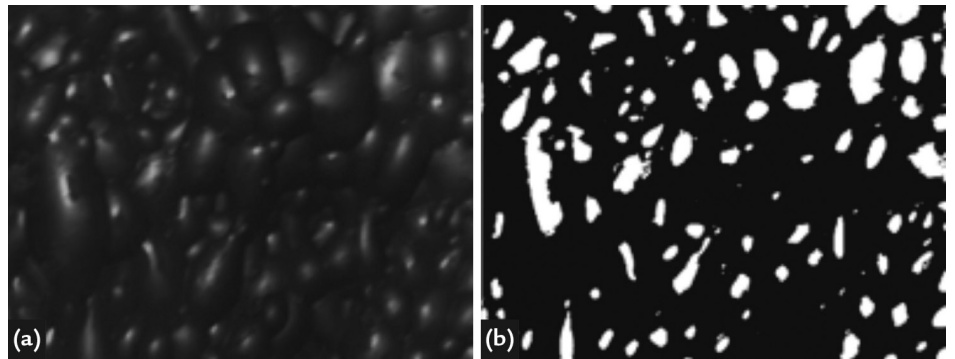


In figure 4, the grayscale image of the normal froth and its binary image are shown under a single scale and thus the bubble size feature can be obtained

by calculating the size of white areas in the binary image. Due to the multi-scale property of wavelet analysis, different sub-images are obtained after

the wavelet transformation of froth image, each of which denotes different information about the original image at different scales.

Figure 4
Grayscale image and binary image of normal froth
(a) Grayscale image
(b) Binary image

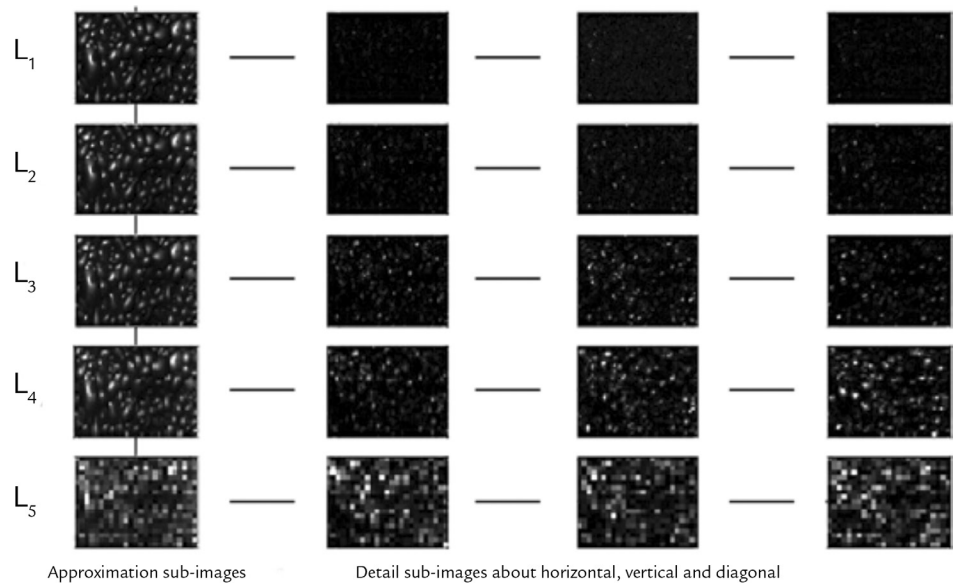


In figure 5, the tree mode for wavelet

decomposition of the normal froth gray-

scale image at level-5 is shown.

Figure 5
Wavelet decomposition of normal froth gray image in tree view mode



It denotes that wavelet multi-scale analysis is essentially the simultaneous analysis of space and frequency of sub-

images at different levels of decomposition; in this way, statistical features can be more informative than the single-scale in-

formation obtained. However, it is hard to directly describe the froth morphological feature based on these traditional features.

3. Equivalent size feature extraction based on wavelet multi-scale binary imagery

At first, the r -level wavelet decomposition of a two-dimensional grayscale image $I_{(X \times Y)}$ is carried out; at each decomposition level, the two-dimensional

wavelet transformation produces an approximation sub-image and three detailed sub-images at horizontal, vertical and diagonal directions respectively.

The wavelet transformation at each decomposition level is as follows:

$$I = \sum_{k,m} c_{k,m}^{j+1} \varphi_{j+1,k,m} = \sum_{k,m} c_{k,m}^j \varphi_{j,k,m} + \sum_{k,m} d_{k,m}^{j,1} \psi_{j,k,m}^1 + \sum_{k,m} d_{k,m}^{j,2} \psi_{j,k,m}^2 + \sum_{k,m} d_{k,m}^{j,3} \psi_{j,k,m}^3 \quad (1)$$

At each decomposition level, the approximation parameter matrix $c_{k,m}^j$ and three detailed parameter matrixes

$d_{k,m}^{j,1}$, $d_{k,m}^{j,2}$ and $d_{k,m}^{j,3}$ can be calculated by the Mallat algorithm for two-dimensional wavelet decomposition, as shown

in the following formula:

$$\begin{cases} c_{k,m}^j = \sum_{l,n} \bar{h}_{2k-l} \bar{h}_{2m-n} c_{l,n}^{j+1} \\ d_{k,m}^{j,1} = \sum_{l,n} \bar{h}_{2k-l} \bar{g}_{2m-n} c_{l,n}^{j+1} \\ d_{k,m}^{j,2} = \sum_{l,n} \bar{g}_{2k-l} \bar{h}_{2m-n} c_{l,n}^{j+1} \\ d_{k,m}^{j,3} = \sum_{l,n} \bar{g}_{2k-l} \bar{g}_{2m-n} c_{l,n}^{j+1} \end{cases} \quad (2)$$

In formula (1) and (2), the scaling function is $\varphi(x, y) = \phi(x)\phi(y)$, and the three wavelet functions are:

$$\psi^1(x, y) = \phi(x)\psi(y), \psi^2(x, y) = \psi(x)\phi(y)$$

$$\text{and } \psi^3(x, y) = \psi(x)\psi(y) \text{ in which}$$

$$\phi(t) = \sqrt{2} \sum_i h_i \phi(2t-i) \quad \psi(t) = \sqrt{2} \sum_i g_i \psi(2t-i)$$

Formula (1) is firstly used for the first level of a two-dimensional wavelet transformation to obtain an approximation sub-image and three detailed sub-images, coefficients of which are calculated through formula (2). And then formula (1) is used for the level-2 two-dimensional wavelet transformation of the first level approximation sub-image (low-frequency part) $c_{k,m}^j$ which produces a level-2 approximation sub-image and three detailed sub-images. The process then is repeated till the wavelet transformation of $c_{k,m}^{j+1}$ at r level is done and

respectively show the two-scale equation and wavelet equation in a one-dimensional perpendicular multi-resolution analysis; the decomposition level $j = r, r-1, \dots, 1, k, m \in \mathbb{Z}$ respectively represents the rows and columns in the parameter matrix $c_{k,m}^j$, and $l, n \in \mathbb{Z}$ respectively represents the rows and columns in parameter matrix $c_{l,n}^{j+1}$.

The coefficient sequence $h = \{h_i\}$ is a low-pass filter and $\bar{h} = \{\bar{h}_i\}$ is the sequential inversion of h , namely $\bar{h}_i = h_{-i}$, while the coefficient sequence $g = \{g_i\}$ is a high-pass filter and $\bar{g}_i = (-1)^i h_{1-i}$, $\bar{g} = \{\bar{g}_i\}$ is the sequential inversion of g , namely $\bar{g}_i = g_{-i}$.

the multi-scale representation of $I_{(X \times Y)}$ is obtained (Mallat S G, 1989). With the increase of decomposition levels, the wavelet sub-image is becoming smaller. In this case, single-branch reconstruction is needed to produce the sub-image with the same size of the original image and to keep the frequency component of each sub-image; namely only the wavelet coefficient of one sub-image is used for signal reconstruction while the coefficients of the other sub-images at the same level are set as zero. Since the approximation sub-image can reflect

the visual outline of the froth image and the detailed sub-images reflect detailed changes in the froth image, to acquire the bubble size feature, the direction of froth the detailed sub-images at different levels is not considered and can be ignored and as such, only the approximation sub-image needs to be reconstructed. Mark the approximation sub-images at r levels respectively as $S^V (v = 1, 2, \dots, r)$ which represent the outline part of froth sub-image at different scales, with the corresponding coefficient sequence being as follows:

$$c_{k,m}^{j+1} = \sum_{l,n} h_{k-2l} h_{m-2n} c_{l,n}^j + \sum_{l,n} h_{k-2l} g_{m-2n} d_{l,n}^{j,1} + \sum_{l,n} g_{k-2l} h_{m-2n} d_{l,n}^{j,2} + \sum_{l,n} g_{k-2l} g_{m-2n} d_{l,n}^{j,3} \quad (3)$$

According to the Uncertainty Principle (Vetterli M, 1995), the space and frequency window areas in wavelet

multi-scale analysis have the invariance property.

Uncertainty Principle $f(x)$ If we

$$\Delta_x^2 = \int_{-\infty}^{+\infty} x^2 |f(x)|^2 dx \quad (4)$$

$$\Delta_\omega^2 = \int_{-\infty}^{+\infty} \omega^2 |F(\omega)|^2 d\omega \quad (5)$$

If a unit energy signal $f(x)$ vanishes faster than $\frac{1}{x^2}$ as $x \rightarrow \infty$, then the product

of the signal durations is greater than or equal to $\pi/2$.

$$\Delta_x^2 \Delta_\omega^2 \geq \frac{\pi}{2} \quad (6)$$

Therefore, the bandwidth of each restructured sub-image corresponds respectively to a different space width. In general, a signal with high frequency decays fast and correspondingly, a narrow space and wide frequency window

are needed for its decomposition, while a signal with low frequency decays slowly and correspondingly, a wide space and narrow frequency window are needed for its decomposition. In this way, large-sized froth size can be rec-

ognized by a wideband wavelet at low frequency and small-sized froth can be recognized by a narrowband wavelet at high frequency; namely, different sizes of froth can be identified by wavelet multi-scale analysis.

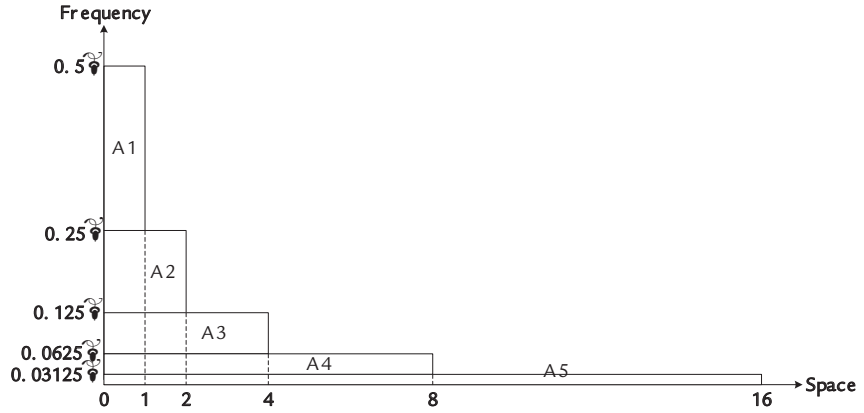


Figure 6 Relationship between space and frequency

Reference (Bharati M.H et al., 2004, SUN Y K,2012) gives the relationship between the frequency domains of signals at different scales. As shown in Figure 6, this space-frequency chart tells us the resolutions of the wavelet, based on space and frequency domains. Due to scaling, the wavelets used in the decomposition have varying space and frequency resolutions, and the frequency duration goes up by 2^j while the spatial duration goes down by 2^j and vice versa. In Figure 6, A1-A5 respectively represent the approximation sub-images at different decomposition scales according to the space-frequency relationships between differently-scaled discrete signal wavelet and the Uncertainty Principle. Assume

$$(7)$$

Since the bubble shape is similar to a circle, its area can be calculated by $p(D_q/2)^2$, D_q whereby is set as the average range of the bubble di-

by using the ‘sym’ wavelet function and that the froth grayscale image is a one-dimensional signal with a frequency range of $0 \sim p$, then based on Uncertainty Principle and Figure 6, it can be seen that the frequency ranges for r reconstructed sub-images are respectively $0 \sim 0.5p$, $0 \sim 0.25p$, ..., $0 \sim p/2^r$ and the corresponding space widths are respectively $0 \sim 1.0 \sim 2$, ..., $0 \sim 2^{r-1}$. If we threshold a sub-image, then only the parts of the sub-image corresponding to the valleys between the bubbles will be removed and most of the other parts of the bubbles will remain. The area of the remaining parts can be thought of as the total area of bubbles with sizes corresponding to the sub-image. After the relationship of

$$E_q = A_{q+1} - A_q, q = 1, 2, \dots, r - 1$$

iameter change, which is respectively $1.5, 3, \dots, 3^i 2^{r-3}$. Then formula (13) is used to calculate the number of bubbles at each level, based on which, N_q is the

$$(8)$$

$$N_q = \frac{E_q}{p(D_q/2)^2}$$

the spatial frequency between the different approximation sub-images is identified, the Otsu method (Otsu N,1979) is adopted for multi-scale binary processing for r in the reconstructed sub-images, namely S' , so as to obtain the multi-scale feature. Then, S' is further binarized to obtain r binary images. Afterwards, the total bubble area, namely the size of white areas in every binary image, is set as A_v . By subtracting the total bubble area of adjacent images, the equivalent size of sub-image, E_q can be obtained. Finally, E_q is the equivalent size feature obtained through the multi-scale binary process and it corresponds to the successive range of bubble diameter change: $1 \sim 2, 2 \sim 4, \dots, 2^{r-2} \sim 2^{r-1}$.

distribution of equivalent size for froth image and can be encountered as follow:

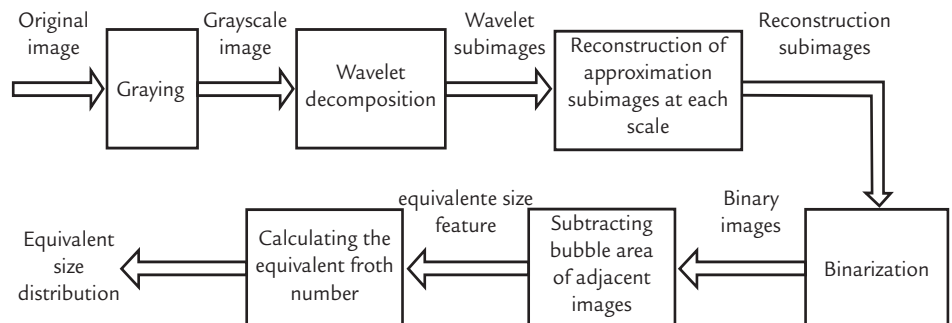


Figure 7 Block diagram for extraction of froth image equivalent size feature

Figure 7 shows the process for extracting the equivalent size feature from the froth image, based on wavelet

Step 1: Make level- r wavelet decomposition of grayscale image $I_{(X \times Y)}$ according to formula (1). At each decomposition level, the two-dimensional wavelet produces an approximation sub-image and three detailed sub-images at horizontal, vertical and diagonal directions respectively.

Step 2: Ignore detailed sub-images at each level and perform single-branch

multi-scale binary imagery.

In conclusion, the steps for extracting from the froth image, the equivalent

reconstruction of the approximation sub-images at each level according to formula (3) so as to obtain the reconstructed sub-image $S^V (v=1,2,\dots,r)$.

Step 3: The approximation sub-images S^V are binarized based on the Otsu method, and then the total froth area A_v of each binary image is worked out.

Step 4: Work out the equivalent size feature of froth, $E_q (q=1,2,\dots,r-1)$,

size feature based on wavelet multi-scale binary imagery are as follows:

according to Formula (7).

Step 5: Calculate the equivalent average diameter of froth, D_q , at different levels according to Figure 6 and the Uncertainty Principle and work out the equivalent froth number N_q according to Formula (8); based on N_q , the equivalent size distribution of froth image can be achieved.

4. Fault condition detection for copper flotation based on the equivalent size feature of a froth image

In online detection of the fault condition for copper flotation based on wavelet multi-scale binary imagery of the froth, there are mainly three steps:

Step 1: Select a number of clear normal-condition froth images and work out the equivalent size feature of each image offline.

Step 2: Combine all the equivalent size distribution diagrams for normal froth images into one and after perform-

ing statistical analysis, determine the minimum and maximum value for each equivalent size feature.

Step 3: Acquire the online equivalent size distribution of the real-time froth image and compare it with the equivalent size distribution feature for normal froth obtained in Step 2. According to previously determined criterion, the production condition corresponding to the real-time froth image is identi-

fied so as to detect any fault condition in time.

The criterion is set as follows: when the number corresponding to each average diameter in the equivalent distribution size for the real-time froth image falls into the range of the equivalent distribution size for the normal froth image, the production condition is considered as normal; otherwise the flotation is considered as under a fault condition.

5. Experiment and analysis

5.1 Equivalent size feature extraction for normal froth image

Collect the froth videos that include the different working conditions under the same feeding conditions as shown in Table 1, which should then be classified by an expert. For this study, 1200 froth images corresponding to the "normal" condition were selected in order to extract the equivalent distribution size, i.e. obtain the minimum and maximum frequencies of all the bubbles with an equivalent diameter.

Firstly, the normal-condition froth

grayscale image from the flotation site is used for the 5-level wavelet decomposition, after which, 5 approximation sub-images (A1~A5) are obtained, The spatial frequency relationship between the different sub-images is shown in Figure 6.

Secondly, the approximation sub-images at each level are binarized and the total froth area of each reconstructed binary image is calculated, so as to obtain the equivalent froth size

feature. The froth number corresponding to each equivalent diameter average is worked out according to Formula (13) and Figure 6, and thus the equivalent size distribution for each reconstructed sub-image of the normal froth image is obtained. Afterwards, different equivalent size distribution diagrams are combined into one for statistical analysis, and the equivalent size distribution for the normal froth image is obtained as shown in Figure 8.

| | feeding ore grade (GCu) | concentration (%) | pH value | particle size(%) |
|-----|-------------------------|-------------------|----------|------------------|
| min | 0.85 | 25 | 10 | 65 |
| max | 1.12 | 32 | 12 | 70 |

Table1
The feeding ores condition

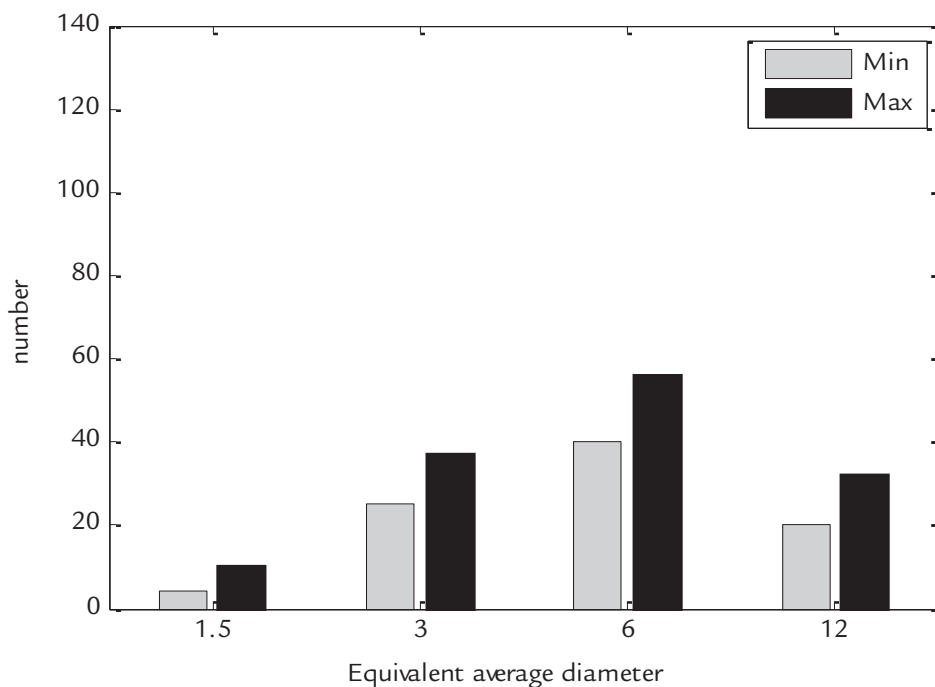


Figure 8
Equivalent size
distribution of normal froth image

5.2 Fault condition detection for copper flotation

Fault conditions detected at the flotation site are greatly different from the normal condition. In the case of viscous froth, the number of large bubbles is relatively low while that of small bubbles is relatively high; while the size distribution of hydrated bubbles is mainly concentrated in the small-size range.

Collected were 600 froth images including “normal” and “fault” working conditions, which is the test data set $D_{(600, 4)}^c$. Firstly, upon expertly classifying the test set of 600 roughing froth images there were 280 “normal” condition froth images 180 “fault” condition hydrated froth images, and 140 viscous froth im-

ages. Then, extract the equivalent size features of each piece of froth image and detect the working condition based on the criterion. As shown in Figure 9 the equivalent size distributions correspond to the froth images of two types fault conditions, namely hydrated froth and viscous froth, which respectively corresponding to the “black” and “gray” legend. According to the predetermined criterion, the number corresponding to the equivalent size feature of hydrated and viscous froth images falls out of the normal range; therefore, the two conditions can apparently be determined as fault conditions.

In a word, through the comparison

between the equivalent distribution size of the normal froth and that of the real-time froth on the basis of predetermined criterion, detection of the flotation condition can be realized in real time. If the fault condition is determined, relevant adjustment of the production operation should be made to ensure that the overall production process is kept at the optimal condition.

The experimental results are shown in Table 2. Among them the recognized accuracy rate of the hydrated froth images is 96.7% the average recognized accuracy rate of the hydrated froth images and normal images is 91.15%.

| | normal froth images | hydrated froth images | viscous froth images |
|-----------------------|---------------------|-----------------------|----------------------|
| Expert classification | 280 | 180 | 140 |
| System classification | 254 | 174 | 152 |
| Error numbers | 26 | 6 | 22 |
| The accuracy rate | 90.8% | 96.7% | 91.5% |

Table2
Working condition
detection results based
on equivalent distribution size feature

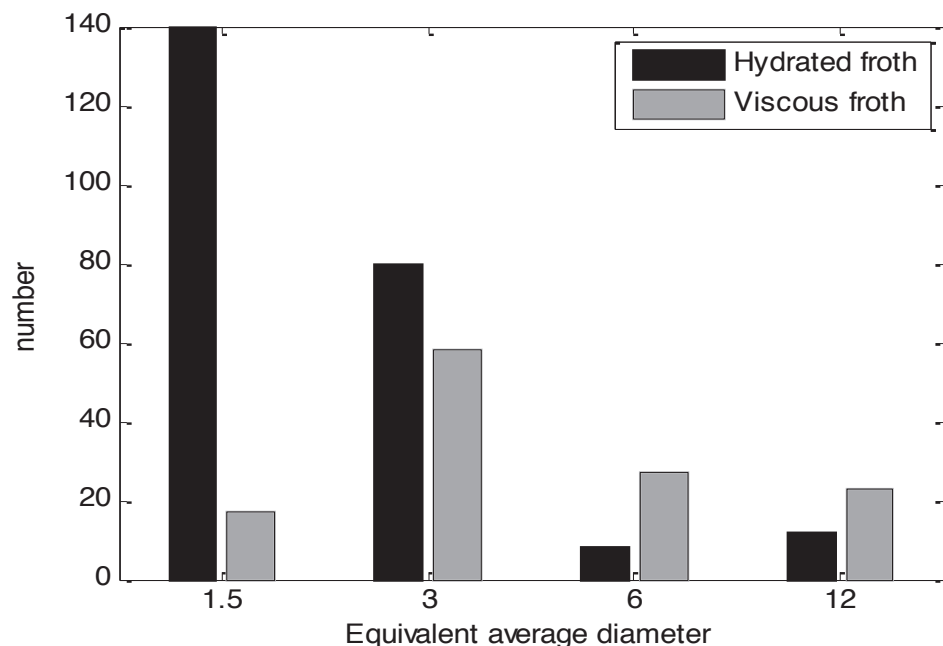


Figure 9
Equivalent size distributions
of froth images of fault condition

6. Conclusion

In fault condition detection, extraction of the morphological feature from the froth image is a vital step. With regards to the froth imagery of copper flotation, this paper proposes that the wavelet multi-scale binary process can be adopted for extraction of the equivalent size feature from the froth image, and that this feature can be used as the basis for fault condition detection in copper flotation. Unlike the traditional feature

extracted by wavelet multi-scale analysis, the equivalent size feature is an effective representation of the original image at different scales. This feature is directly related to froth surface morphology and has a multi-scale property; therefore, it can capture the morphological feature more informatively than the single-scale feature. Based on the experiment with real froth images acquired at the flotation site, it is shown that the wavelet multi-scale binary

method for extraction of the equivalent size feature proposed in this paper, together with the fault condition detection method that compares the equivalent size distribution of the real-time froth image with that of the normal image, can detect the fault condition in copper flotation in a direct and simply manner. Therefore, these two methods are of relatively great theoretical significance and can be promoted in practice.

7. Acknowledgements

The authors gratefully acknowledge the support from Science Fund for Creative Research Groups of the National

Natural Science Foundation of China (Grant no:61321003), National Natural Science Foundation of China (Grant nos:

61273169, 61134006), support from the Science and Technology Plan Foundation of Hunan Province (2014GK3011).

9. References

- ALLDRICH, C; MAIIAAS, C, SHEAN, B. J. Online monitoring and control of froth flotation systems with machine vision: a review. *International Journal of Mineral Processing*, p.961-13,2010.
- BHARATI, M.H; MacGregor, J.F. Image texture analysis: methods and comparisons, *Chemometrics and Intelligent Laboratory Systems*, v.72,p.57-71,2004.
- BAO, L; BODIL, R. Bubble size estimation for flotation processes. *Minerals Engineering*, v.21 ,p.539-548,2008.
- BARTOLACCI, G; PELLETIER, R., TESSIER. J. Application of numerical image analysis to process diagnosis and physical parameter measurement in mineral processes —Part I: Flotation control based on froth textural characteristic. *Minerals Engineering*,v.19,p.734-747,2006.
- CIT, I. R. C; AKTAS, Z; BER, BERR. Off line image analysis for froth flotation of coal. *Computers & Chemical Engineering*, v.28,p.625-632,2004.
- GUI, W, H; YANG, CH, H; LU, M. et al. Machine-vision-based online measuring and controlling technologies for mineral flotation-a review[J]. *Acta Automatica Sinica*, 2013, 39(11):1879-1887.
- PARTS-MONTALBAN, J.M., JUAN, A. de., FERRER, A. Multivariate image analysis: a review with applications. *Chemometrics and Intelligent Laboratory*

- Systems, v.107, n.1, p.1-23, 2011.
- LIN, Y. Q.; YANG, CH. H., HE M.F. Fault condition detection for sulfur flotation process based on texture unit distribution. *Computing Technology and Automation*, v.32, p.31, 2013.
- LIU, J. J., MACGREGOR J. F., DUCHESNE C. Flotation froth monitoring using multiresolutional multivariate image analysis. *Minerals Engineering*, v.18, p.65-76, 2005.
- MOOLMAN, D.W., ALDRICH, C., VAN DEVENTER, J. S. J., STRANGE, W.W. Digital image processing as a tool for on-line monitoring of froth in flotation plants [J]. *Miner. Eng.*, 1994, v. 7, n. 9, p. 1149-1164.
- MOOLMAN, D.W., ALDRICH, C., VAN DEVENTER, J. S. J., BRADSHAW, D.J. 1995b. The video graphic characterization of flotation froths using neural networks. *Chemical Engineering*. v.50 ,p.3501-3513, 1995.
- MALLAT, S, G. A theory for multiresolution signal decomposition: the wavelet representation. *IEEE Transactions on Pattern Analysis and Machine Intelligence*, v.11, p.674-693, 1989.
- OTSU, N. A threshold selection method from gray level histogram [J]. *IEEE Transactions on Systems Man, and Cybernetics*, v.9, p.62-66, 1979.
- REN, H. F., YANG, CH. H., ZHOU, X. et al. Froth image feature weighted SVM based working condition recognition for flotation process. *Journal of Zhejiang University*, v.45, n.12, p.2115-2119, 2011.
- SUN, Y. K. *Wavelet transform and image graphics processing technology*. Bei Jing: Tsinghua University Press, p.146-147, 2012.
- TANG, ZH. H., SUN, Y. Y. Flotation froth image texture feature extraction based on wavelet transform. *Computer Engineering*, v.37, p.206-208, 2011.
- VETTERLI, M., KOVACEVIC, J. *Wavelets and Subband Coding*. Englewood Cliffs: Prentice Hall, 1995.
- XU, C. H., GUI, W. H. YANG, CH. H. Flotation process fault detection using output PDF of bubble size distribution. *Minerals Engineering*. v.26, p.5-12, 2012.
- YANG, CH. H., ZHOU, K. J., MU, X. M. et al. Froth color and size measurement method for flotation based on computer vision. , *Chinese Journal of Scientific Instrument*, v.30, n.4, p.717-721, 2009.
- YANG, CH. H., XU, C. H., GUI, W. H. Application of high light removal and multivariate image analysis to color measurement of flotation bubble images. *International Journal of Imaging Systems and Technology*, v.19, p.316-322 , 2009.

Received: 20 October 2014 - Accepted: 25 January 2015.